A 4:1 Dual-Polarized Connected Array Prototype with Parallel Plate Waveguide Feeds

R. Ozzola[#], U. Imberg[$], D. Cavallo[#]

[#]Terahertz Sensing Group, Delft University of Technology, The Netherlands
[$]Huawei Technologies AB, Sweden
{r.ozzola-1, d.cavallo}@tudelft.nl, ulrik.imberg@huawei.com

***Abstract*— A dual-polarized ultra-wideband array prototype operating from 2 to 8 GHz is designed, manufactured, and tested. The array consists of 8×16 connected slot elements per polarization, with artificial dielectric layers placed above the slots. The design exploits a feed concept based on parallel plate waveguides, with the goal of improving the manufacturability of the printed circuit board realizing the array. One-to-eight corporate feeding networks are also designed to reduce the number of coaxial connectors. Measured results of the matching and radiation performance are shown to be in good agreement with simulated predictions.**

***Keywords*— phased arrays, printed circuit board, mobile communications, ultrawide-band arrays.**

I. Introduction

Massive Multiple-Input Multiple-Output (MIMO) systems are the prominent enablers of high-data rate communications for the next generation of mobile communications [1]. Specifically, the use of multi-beam phased arrays for wireless base stations provides several benefits in terms of flexibility, higher user capacity, dynamic coverage, and reduced interference. Moreover, multiple frequency bands will be employed at either microwave or millimeter wave frequencies. Therefore, wideband and wide-scanning phased arrays are sought to generate links over a wide field of view and to integrate multiple frequency bands in the same antenna aperture [2]–[4].

In [4], an example of wideband array for base station systems was presented. It consisted of a dual-polarized connected slot array antenna with an artificial dielectric layer (ADL) radome for sub-8 GHz applications. Despite the good performance, the manufacturing of the array with printed circuit board technology presented several critical aspects due to mechanical and thermal issues. The manufacturing complexity was linked to the integrated coaxial lines implementing the feeding structure, requiring blind and thin vias, and to the milling of the substrate needed to reduce its effective permittivity and avoid scan blindness [5].

In [6], [7], an alternative feed based on a parallel-plate waveguide (PPW) was proposed. This constitutes an easier solution as the feed design is decoupled from the radiating section, and vias with a smaller aspect ratio can be employed. In this contribution, we improve the design of [4] by using the PPW feed, avoiding dielectric perforations in the substrate, and implementing a hybrid feeding network with each array column of 8 elements fed by one connector. The design uses the same ADL radome of [4] to cover the 2-8 GHz band. A 16×8 array prototype is developed and tested to demonstrate the advantage of this design in terms of manufacturability. The measured impedance and radiation performance are shown to be in good agreement with simulations.

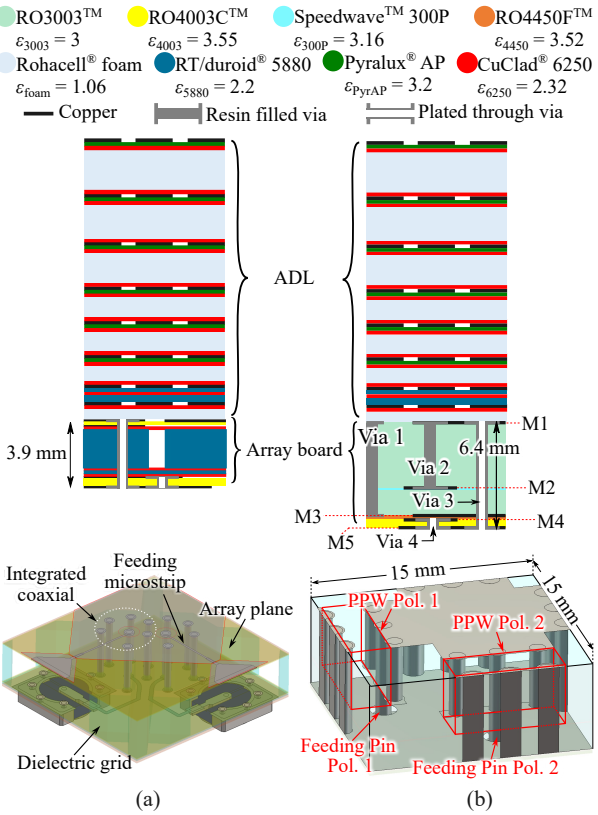

Fig. 1. Comparison between the (a) coaxial-fed [4] and (b) PPW-fed unit cell, considering the stackups (top) and the 3D views of the unit cells (bottom).

II. Array Design

A. Unit Cell Design

The design of the connected slot array in [4] consisted of an ADL radome with eight metal layers, implementing a wideband impedance transformer, and dual-polarized 45° tapered radiating slots, as shown in Fig. 1(a). The slots are fed with microstrip lines terminated with a capacitive plate, connected to an integrated coaxial line made of vias. The manufacturing of these vias is not trivial due to the large

Table 1. Detailed description of the board stackup including the metal layers, dielectric substrates and vias.

Metal layer	Function	Dielectric	Thickness [µm]
M1	Radiating plane		18
		RO3003™	4060
M2	Pads		18
		Speedwave™ 300P	51
		RO3003™	1905
M3	Ground plane		18
		RO4450F™	102
M4	Capacitive pads		18
		RO4003C™	203
M5	Feeding network		18
		Total	6415

	From	To	Type	Diameter [µm]
Via 1	M1	M3	Resin filled	1.4
Via 2	M1	M2	Resin filled	1.1
Via 3	M1	M5	Plated through	1.1
Via 4	M4	M5	Plated through	0.4

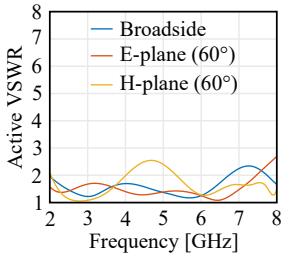

Fig. 2. Active VSWR of the unit cell for broadside and scanning to 60° on the main planes.

aspect ratio required to keep the size of the two coaxial lines (one per polarization) compact. Another coaxial-to-microstrip transition is placed below the ground plane to reach the coaxial connectors. The dielectric substrate is perforated to lower its effective permittivity and avoid scan blindness for large scan angle. This comes at the cost of increased manufacturing complexity, due to mechanical and thermal properties of multi-stack layers with embedded cavities.

An alternative design proposed here is shown in Fig. 1(b). The same ADL radome is used, but the radiating part is altered by employing the PPW feed concept described in [6]. The unit cell period is $15\,\mathrm{mm}$, and its stackup is described in Table 1. Each polarization is fed with a pin, which connect to the slot located on the layer M1 through a PPW line located on one side of the pin. On the opposite side, both polarizations share a cavity. The PPW and cavity walls are realized through vias, with a maximum aspect ratio of 4.6, which eases the manufacturing. For this design, differently from the other prototype, no milled dielectrics are used.

The unit cell yields the active Voltage Standing Wave Ratio (VSWR) in Fig. 2, which is lower than 2.3 at broadside and 2.6 when scanning to $60°$ in the main planes.

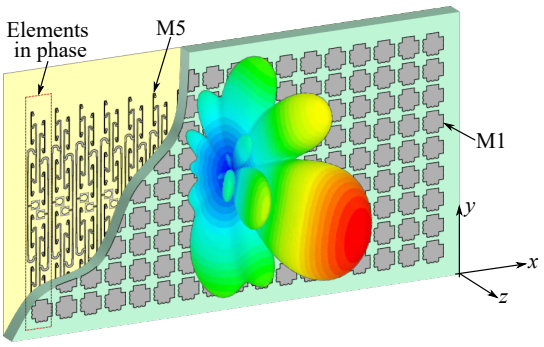

Fig. 3. Sketch of the array concept without the ADL radome, where the elements of the same column are fed in phase with an 8-to-1 corporate feeding network, allowing a beam steering capability on the xz-plane.

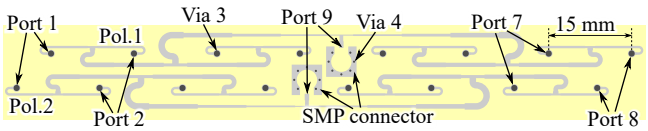

Fig. 4. View of M5, where the 1-to-8 corporate feeding networks of both polarizations are printed.

B. *Corporate Feeding Network and Finite Array*

The targeted array prototype comprises 16×8 elements per polarization, where each column is fed by a 1-to-8 corporate feeding network, as shown in Fig. 3. With this feeding solution only scanning in the xz-plane is allowed by combining the embedded pattern. However, since two polarizations are fed, scanning in both E- and H-plane is achieved.

The feeding network is located on M5, and it uses M3 as the ground plane [see Fig. 1(b) and Table 1]. The three-stage feeding network is shown in Fig. 4, and it connects the feeding pins to the $50\,\Omega$ SMP connector of port 9. The matching at the input port, i.e., port 9, is shown in Fig. 5(a) exhibiting values lower than $-16\,\mathrm{dB}$. The maximum variation of the coupling between the input and the output ports are shown in Fig 5(b) in terms of amplitude and phase, being smaller than $0.55\,\mathrm{dB}$ and $13°$, respectively. Finally, the losses are shown in Fig 5(c).

The matching of the array connected to the feeding network is shown in Fig. 5(d), where an $8\times\infty$ array simulation is considered. It exhibits an active VSWR lower than 2.6 at broadside, lower than 2.8 and 3 when scanning to $60°$ in the H- and E-plane, respectively.

III. Prototype and Measurements

The 16×8 array board prototype is shown in Fig. 6(a) and (b), at the back and front, respectively. The array is combined with a mounting frame and the ADL radome, as shown in Fig. 7.

A. *Active Matching*

The S-parameters of the 8th column for both polarizations [see Fig. 7(a)] are measured to characterize their active matching. The resulting active VSWR is shown in Fig. 8. The active matching at broadside is shown in Fig. 8(a) for both polarizations, yielding values lower than 2.8. The scanning

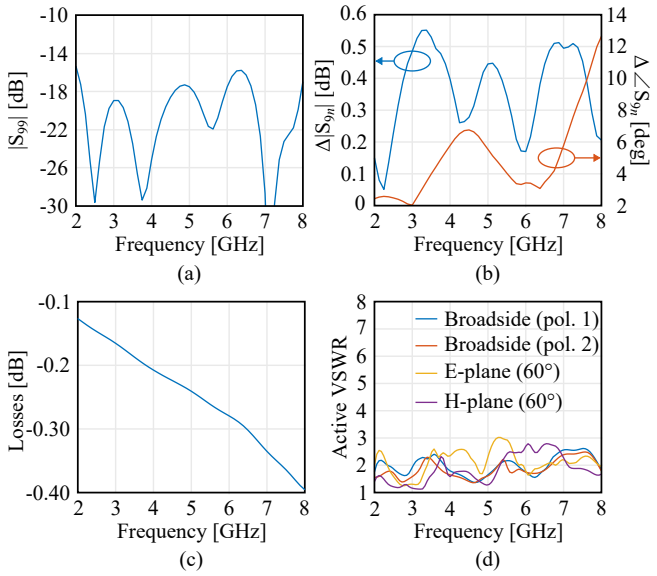

Fig. 5. (a) Input reflection coefficient of the feeding network (expressed as $|S_{99}|$), (b) deviation of S_{9n} in terms of amplitute and phase, (c) losses of the feeding network, (d) active VSWR of the $8 \times \infty$ connected array combined with the feeding network.

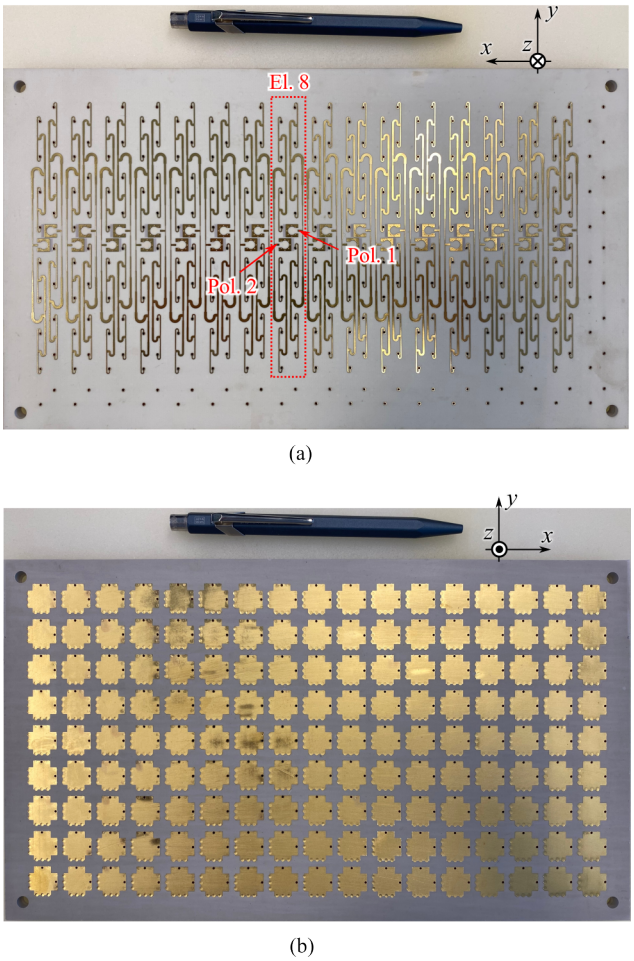

Fig. 6. (a) Back and (b) front view of the array board.

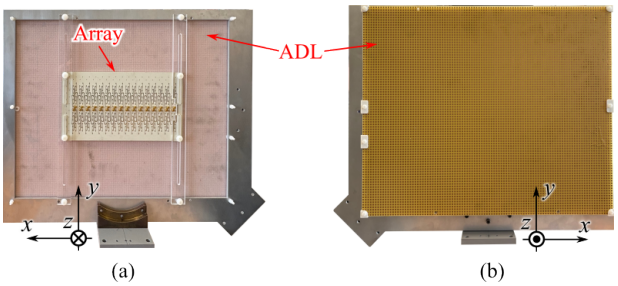

Fig. 7. (a) Back and (b) front view of the prototype together with the ADL and the antenna holder.

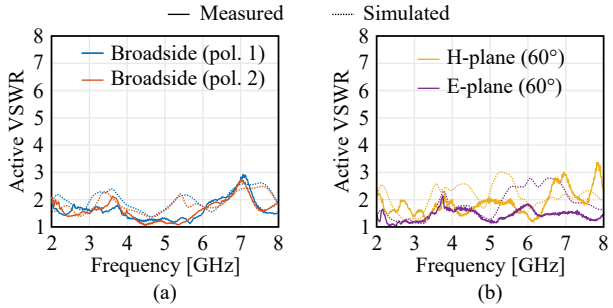

Fig. 8. Comparison of the measured and simulated Active VSWR for (a) broadside and (b) scanning.

performance is reported in Fig. 8(b), exhibiting VSWR values lower than 3.3 and 2 between when scanning to 60° in the H- and E-plane, respectively, i.e., when steering the beam on the xz plane. Simulated results from an $8 \times \infty$ array simulation are also reported in the figure for comparison.

B. Far-Field Patterns

The far-field patterns are measured on the xz-plane for all the 16 elements of both polarizations and on the yx-plane for element 8 of both polarizations.

The embedded element patterns (EEPs) of all the elements measured on the xz-plane are combined to form the array patterns, as shown in Fig. 9. Co-polar and cross-polar patterns are reported at three different frequencies within the band of operation and for several scanning conditions in the range from $-60°$ to $60°$. The patterns are normalized to the broadside co-polar value. The asymmetries in the side lobes, present especially when scanning, are due to the asymmetry of the antenna board [see Fig. 7(a) and (b)]. A larger scan loss is observed in Fig. 9(c) for polarization 1, which can be attributed to a higher mismatch at 8 GHz when scanning in the H-plane, as shown in Fig. 8(b).

Fig. 10 shows the measured patterns on the yz plane of element 8 of both polarizations. These patterns are created through the in-phase excitation of eight elements with the corporate feeding network.

C. Considerations on the Cross-Polarization

The cross-polar levels of the array, which can be seen in Fig. 9 and 10, are intrinsically high due to the unit cell design. As it can be seen in Fig. 1(b), the two feeding pins share the

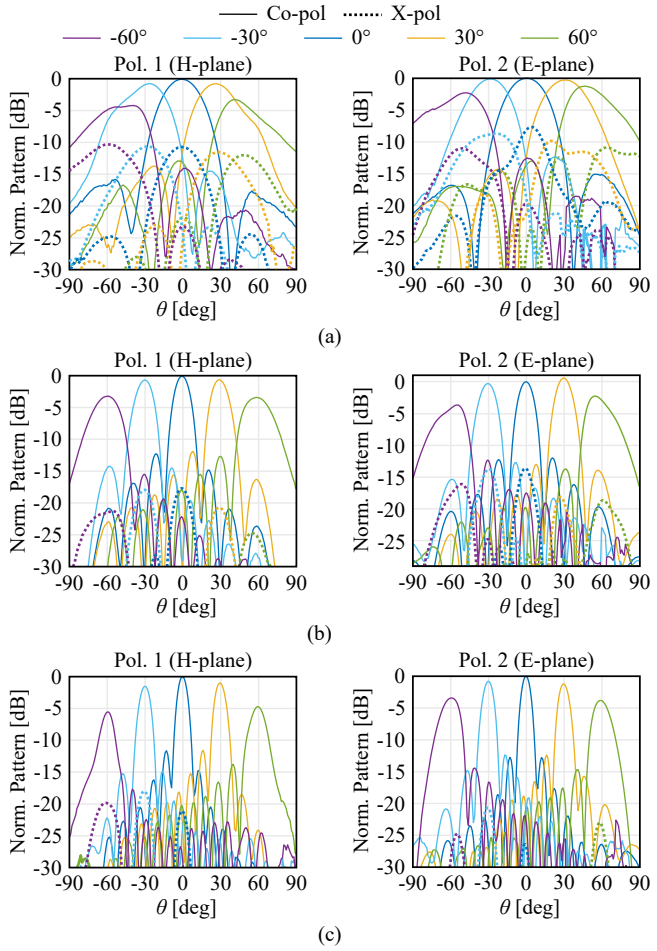

Fig. 9. Co- and cross-polar normalized patterns measured on the xz-plane at (a) 2 GHz, (b) 5 GHz, and (c) 8 GHz for different scanning configurations.

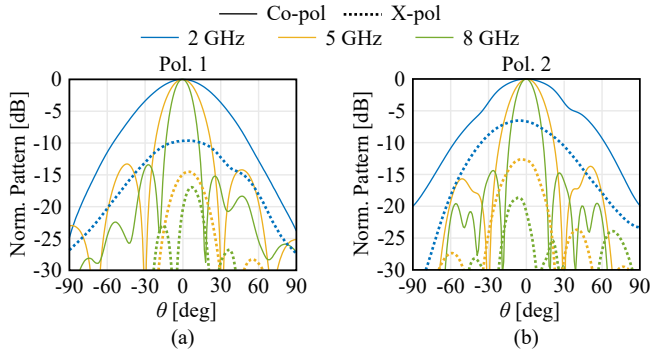

Fig. 10. Co- and cross-polar normalized patterns measured on the yz-plane for element 8 of (a) polarization 1 and (b) polarization 2 at different frequencies.

same cavity, allowing the two polarizations to couple. This effect is shown in Fig. 11(a) in terms of $|S_{12}|$ between the orthogonal slots in the unit cell, assuming broadside scanning. The mutual coupling is higher than $-10\,\mathrm{dB}$ at low frequency. Nevertheless, the cross-polar rejection can be improved by using the two polarizations simultaneously in such a way that one set of slots is fed with the amplitude which cancels the the cross-polar component of the orthogonal slots in a

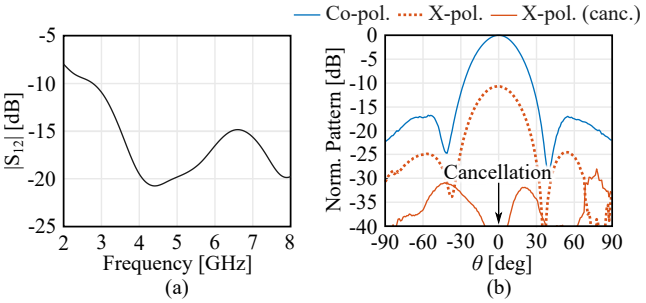

Fig. 11. (a) Simulated $|S_{12}|$ for the unit cell and (b) study on the cross-pol cancellation at 2 GHz at broadside.

certain direction at a certain frequency. To show the feasibility of this concept, the patterns of polarization 1 at 2 GHz on the xz-plane are considered in Fig. 11(b). The intrinsic $-10\,\mathrm{dB}$ cross-polar rejection is improved by combining the two polarizations with the proper weights. For the present case, as shown in Fig. 11(b), this operation is done to cancel the cross-polarization at broadside at 2 GHz. Although a perfect cancellation is achieved at broadside, lower cross-polar levels are obtained for all directions.

IV. Conclusion

A dual-polarized connected slot array was developed for wideband operation in the 2-8 GHz band. The radiating part of the array uses a simplified feed strategy based on parallel plate waveguides to reduce the manufacturing complexity. The resulting printed circuit board does not require perforations in the substrate and uses three dielectric slabs with large diameter vias. Measured results for the active impedance, radiation patterns and cross-polarization levels were presented, proving the viability of the design.

Acknowledgment

This work was supported by HUAWEI Technologies Sweden AB, UNB Project, under Grant YBN2020045031.

References

[1] E. G. Larsson, O. Edfors, F. Tufvesson, and T. L. Marzetta, "Massive MIMO for next generation wireless systems," *IEEE Commun. Mag.*, vol. 52, no. 2, pp. 186–195, 2014.

[2] D.-M. Sun, Z.-C. Hao, W.-Y. Liu, and C.-Y Ding, "An ultrawideband dual-polarized phased array antenna for sub-3–GHz 5G applications with a high polarization isolation," *IEEE Trans. Antennas Propag.*, vol. 71, no. 5, pp. 4055–4065, 2023.

[3] T.-L. Zhang, L. Chen, S. M. Moghaddam, A. U. Zaman, and J. Yang, "Millimeter-wave ultrawideband circularly polarized planar array antenna using bold-C spiral elements with concept of tightly coupled array," *IEEE Trans. Antennas Propag.*, vol. 69, no. 4, pp. 2013–2022, 2021.

[4] R. Ozzola, A. Neto, U. Imberg, and D. Cavallo, "Connected slot array with interchangeable ADL radome for sub-8 GHz 5G applications," *IEEE Trans. Antennas Propag.*, vol. 72, no. 1, pp. 992–997, 2024.

[5] A. J. van Katwijk, "Analysis and design of wideband phased arrays for Ku- and Ka-band satcom applications," PhD thesis, Faculty of EEMCS, Delft Univ. of Technology, Delft, The Netherlands, 2024.

[6] D. Cavallo, "Parallel-plate waveguide-feeding structure for planar-connected arrays," *IEEE Antennas Wireless Propag. Lett*, vol. 21, no. 4, pp. 765–768, 2022.

[7] C. M. Coco Martin and D. Cavallo, "Equivalent circuit representation of a parallel plate waveguide fed connected array," *IEEE Trans. Antennas Propag.*, vol. 73, no. 3, pp. 1496–1504, 2025.